PFC/JA-96-27

X-ray Observations of Up-Down Impurity Density Asymmetries in Alcator C-Mod Plasmas

J.E. Rice, J.L. Terry, E.S. Marmar, F. Bombarda[1]

August 1996

[1]Associazione ENEA-Euratom per la Fusione, 00044 Frascati, Italy.

Submitted to Nuclear Fusion.

This work was supported by the U. S. Department of Energy Contract No. DE-AC02-78ET51013. Reproduction, translation, publication, use and disposal, in whole or in part by or for the United States government is permitted.

X-ray Observations of Up-Down Impurity Density Asymmetries in Alcator C-Mod Plasmas

J.E.Rice, J.L.Terry, E.S.Marmar and F.Bombarda†

Plasma Fusion Center, MIT, Cambridge, MA 02139-4307

† *Associazione ENEA-Euratom per la Fusione, 00044 Frascati, Italy*

Abstract

A five chord, high resolution x-ray spectrometer array has been used to measure vertical brightness profiles of heliumlike argon emission from Alcator C-Mod plasmas, out to the last closed flux surface. During standard Alcator C-Mod operation, with the X-point and the ion $\mathbf{B}\times\nabla\mathbf{B}$ drift down, the heliumlike argon brightness is a factor of ~8 larger at the top of the plasma than at the bottom, near the plasma edge. In these edge regions, where the electron temperature is low, upper levels of observed transitions are populated by radiative recombination of hydrogenlike argon. This up-down brightness asymmetry can be explained by a factor of ~8 enhancement of hydrogenlike argon at the top of the machine at r/a = .9 . This implies a vertical impurity drift from inside the plasma since the hydrogenlike argon is born near the plasma center. With the ion $\mathbf{B}\times\nabla\mathbf{B}$ drift up, the enhancement switched to the bottom of the machine, but did not change when the X-point was moved up. This asymmetry agrees qualitatively with the predictions of neo-classical parallel impurity transport.

I. Introduction

There have been several observations of vertical up-down impurity density asymmetries in tokamak plasmas, from Alcator A [1], PDX [2], TEXT [3], COMPASS-C [4] and Phaedras [5]. Most of these are measurements [1,2,4,5] of intrinsic low Z impurities; in Alcator A, PDX and Phaedras, asymmetric radial profiles of individual charge states have been obtained from wavelength resolving UV spectrometers. In TEXT and COMPASS-C, the observations (spectrally unresolved) were from soft x-ray cameras, and the observed x-ray line brightness asymmetries were assumed to be equal to the local impurity density asymmetries. Comparisons have been made between these observations and the predictions of neo-classical impurity transport theory [6,2,7,8]. Only in Ref.[6] were the complete radial profiles of Alcator A compared to the predictions of the linear theory, in the collisional regime. For the PDX observations, comparison [2] with the plateau and banana regime calculations were made at the C V radius, to avoid complications from the edge plasma. Predictions of the non-linear theory [7,8,4] have been compared to the observations of TEXT and COMPASS-C, but at only one radial location, since pertinent diagnostic information, most notably the ion temperature profile, was not available. Nevertheless, in all cases the direction of the observed impurity density asymmetry, opposite to the ion $\mathbf{B}\times\nabla\mathbf{B}$ drift direction, is in agreement with the predictions of neo-classical theory.

In the case of Alcator C-Mod, up-down brightness profiles of the x-ray emission from Ar^{16+} have been obtained, and large up-down brightness asymmetries in the direction opposite to the ion $\mathbf{B}\times\nabla\mathbf{B}$ drift direction have been observed near the plasma edge. Here the upper levels of the lines are populated by radiative recombination of Ar^{17+} which is produced at the center of the plasma and then diffuses out to the edge before recombining, so plasma edge effects are probably not involved in producing the asymmetry. Alcator C-Mod plasmas are well diagnosed so complete radial profiles of relevant plasma parameters are available.

The organization of this paper is as follows: in section II a brief description of

the experiment is given, in section III the observed impurity asymmetries are shown, and in section IV modelling and comparisons with the predictions of neo-classical impurity transport are presented.

II. Experiment Description

The x-ray observations described here were obtained from the Alcator C-Mod [9] tokamak, a compact (a=22.5 cm, R=67 cm, $\kappa \leq 1.8$) high field device with all molybdenum plasma facing components. The spectra were recorded by a five chord, independently spatially scannable, high resolution x-ray spectrometer array [10]. Each von Hamos type spectrometer consists of a variable entrance slit, a quartz crystal (2d=6.687 Å) and a position sensitive proportional counter detector. Each spectrometer has a resolving power of 4500, a 2 cm chordal resolution and a wavelength range from 2.8 to 4.0 Å. Spectra are normally collected every 50 ms during a discharge, with 120 mÅ covered at any one wavelength setting. A typical value of the spectrometer luminosity function is 7 x 10^{-9} cm^2sr, calculated from the crystal reflectivity, spectrometer geometry and Be window transmission. The vertical scanning limits of the spectrometer system are ±32 cm at the plasma nominal major radius. This allows chordal views completely outside the last closed flux surface at the top and bottom of the machine for plasma elongations less than 1.8.

III. Observed Impurity Profiles

Shown in Fig.1 are the time histories of several parameters of interest for an ohmically heated deuterium, $B_T = 5.3$ T discharge. During this particular discharge there was a low density period between .45 and .55 s, and a high density steady state between .85 and 1.05 s. Argon (Z=18) gas was injected in a 35 ms wide pulse through a piezoelectric valve at .4 s. Shown in Fig.2 is an Ar^{16+} x-ray spectrum [11-17] obtained along a centrally viewing chord at .5 s, when the

central electron density was 1.3×10^{14} cm^{-3} and the central electron temperature was 2.35 keV. This spectrum is dominated by the resonance line, w ($1s2p\ ^1P_1$ -$1s^2\ ^1S_0$, 3949.28 mÅ), and the forbidden line, z ($1s2p\ ^3S_1$ -$1s^2\ ^1S_0$, 3994.28 mÅ) and the intercombination lines, x and y ($1s2p\ ^3P_2$ -$1s^2\ ^1S_0$, 3965.99 mÅ, and $1s2p\ ^3P_1$ -$1s^2\ ^1S_0$, 3969.40 mÅ) are prominent. Also visible are several weaker satellite lines. Shown by the thin line in the figure is a synthetic spectrum whose line intensities are equal to the calculated central chord brightnesses, line widths are given the appropriate Doppler broadening for the ion temperature and line wavelengths are taken from Refs.[18,19]. Chordal brightnesses of w, x, y and z are determined from emissivity profiles calculated from the collisional-radiative model of Refs.[20,21], which includes population of the upper levels via collisional excitation of heliumlike Ar^{16+}, radiative recombination of hydrogenlike Ar^{17+} and inner shell ionization of lithiumlike Ar^{15+}. Measured electron density profiles are obtained from the laser interferometer [22], Thomson scattering and reflectometer diagnostics and the electron temperature profiles are from the electron cyclotron emission [23] and Thomson scattering diagnostics. Argon charge state density profiles are calculated from MIST [24], using impurity transport coefficients [25], appropriate for this portion of the discharge, of D=5000 cm^2/sec and V=-222(r/a) cm/sec. The agreement between the measured and simulated spectra is very good. The only free parameter in this comparison is the normalization, which is used to measure the argon density in the plasma. The total argon density time history determined in this way is shown in Fig.1. The central argon density peaks at a value just under 4×10^{10} cm^{-3} during the low density plateau, and then settles to $\sim1\times10^{10}$ cm^{-3}. The total number of injected argon atoms was 1.7×10^{18}, and given a plasma volume of $\sim10^6$ cm^3, the argon penetration (defined as the ratio between the number of atoms in the plasma to the number injected) was around 2.5% [25,26].

Spectra may be obtained along five separate chords during one discharge by the spectrometer system. Shown in Fig.3 are x-ray spectra of Ar^{16+} taken from two chords tangent to the same flux surface (from EFIT [27]) which crosses the plasma midplane at a major radius of 81.2 cm, at .5 s of a discharge similar to

that shown in Fig.1. The plasma center, denoted in the figure by the '+' sign, was located at R=68.1 cm and Z=−.7 cm, so these spectra are both characterized by r=13.1 cm (81.2 cm - 68.1 cm). The vacuum vessel center is shown by the '×'. The individual lines of sight are shown in the inset in the figure, and the spectrum shown by the solid curve was from a view which crosses the vertical plane at R=67 cm at Z=+16.5 cm (solid line), and the dotted spectrum was from Z=−18.0 cm (dotted line). The two spectra are nearly identical in intensity, indicating that the argon x-ray emission along this flux surface is constant. (The mappings of the two lines of sight back to the plasma midplane are shown by the dot and asterisk.) These spectra are quite different from the central chord spectrum of Fig.2, in that the overall intensity is greatly reduced, and all line intensities have grown relative to the resonance line. The lines are narrower than in Fig.2 due to the lower ion temperature at this radius. Also shown in the figure by the thin line is a synthetic spectrum for these viewing chords, again in good agreement with the observed spectra. Spectra obtained from near the last closed flux surface are presented in Fig.4. Shown by the solid curve is a spectrum from along the solid sightline viewing the top of the plasma, characterized by R=89.4 cm, r=21.1 cm and Z=+28.9 cm. This spectrum is dominated by the forbidden line z, as the resonance line has fallen in intensity compared to Fig.3, the satellites have all disappeared, and the lines are all very narrow. This is indicative of a recombining plasma [12,16], where the line population is overwhelmingly dominated by radiative recombination of hydrogenlike Ar^{17+}. The reason that Ar^{17+} exists at this radius, where the electron temperature is ~200 eV, is because of the fast radial (outward) impurity transport, described by D=5000 cm^2/sec. Shown by the dotted curve is a spectrum from along the dotted sightline viewing the bottom of the plasma but near the same flux surface, characterized by R=88.5 cm, r=20.2 cm and Z=−30.9 cm. The brightness of this spectrum is about a factor of 6 lower than the spectrum taken from the top of the plasma. Also shown in the figure by the thin line is a synthetic spectrum for these viewing chords, normalized to the top spectrum, again in good agreement with the observed spectra. The plasmas of Figs.1-4 all had the ion $\mathbf{B}\times\nabla\mathbf{B}$ drift

direction toward the bottom of the machine (plasma current and toroidal field in the clockwise direction from above), and the single null X-point was at the bottom as well. Alcator C-Mod has also been operated with the ion $\mathbf{B}\times\nabla\mathbf{B}$ drift direction toward the top of the machine, by reversing the toroidal magnetic field direction (the plasma current direction was simultaneously reversed). Argon x-ray spectra have been obtained for plasmas with similar discharge conditions as in Fig.1. Shown in Fig.5 by the solid curve is a spectrum from the solid sightline characterized by R=87.4 cm, r=19.5 cm and Z=+25.9 cm, and by the dotted curve from R=87.2 cm, r=19.3 cm and Z=−28.9 cm. In this case, with the ion $\mathbf{B}\times\nabla\mathbf{B}$ drift direction upward, the spectrum from the bottom of the plasma is about a factor of 8 brighter. (The X-point was located in the bottom of the machine for these spectra.) Figs.4 and 5 demonstrate that impurity x-ray emission is not constant on flux surfaces near the edge, and that this large up-down impurity asymmetry is in the direction opposite to that of the ion $\mathbf{B}\times\nabla\mathbf{B}$ drift direction. These results are summarized in Fig.6, where the brightness of the forbidden line is plotted as a function of the vertical distance from the sightline to the vacuum vessel center at R=67 cm. The asterisks were obtained during the low density plateau of a sequence of identical discharges similar to that shown in Fig.1, with the ion $\mathbf{B}\times\nabla\mathbf{B}$ drift direction down. The asymmetry begins at the top of the plasma around +20 cm, and extends out to the last closed flux surface, with a maximum brightness ratio (of the top to the bottom) of about a factor of 10. The points shown as boxes were obtained from a series of discharges with similar conditions, except with the ion $\mathbf{B}\times\nabla\mathbf{B}$ drift direction up, and in this case the asymmetry (enhancement) is at the bottom of the plasma. Similar observations have been made from Alcator C [28] plasmas. Shown in Fig.7 are the resonance and forbidden line brightness profiles for a series of identical Alcator C 8 T, 350 kA hydrogen discharges with T_{e0} = 1400 eV, n_e = $1.8\times10^{14}/cm^3$, a limiter radius of 16.5 cm and with the ion $\mathbf{B}\times\nabla\mathbf{B}$ drift direction up. In this case there is also a large enhancement in the bottom of the plasma. This may explain the underestimate of the calculated brightnesses compared to the observed profiles in the modelling of Ref.[16].

IV. Modelling and Comparison with Neo-classical Theory

In order to calculate the brightness profiles of the forbidden line for comparison with the profiles of Fig.6, the electron temperature and density profiles, and the individual argon charge state density profiles must be known. The electron temperature profile is shown in Fig.8, obtained during the low density plateau of the discharge shown in Fig.1. Also shown in the figure by asterisks is the ion temperature profile, obtained in the sequence of identical discharges, from the Doppler broadening of the argon x-ray lines, along with an analytic fit to the data. For this low density portion of the discharge, the electron temperature is nearly 75% greater than the ion temperature, though the profile shapes are similar. The electron density profile at .5 s is shown in Fig.9, along with an analytic fit. Also shown in the figure is the total argon density ($\times 1000$), calculated from MIST, using D(r) = 5000 cm^2/sec and V(r) = -222 (r/a) cm/s. The calculated individual charge state density profiles for hydrogenlike Ar^{17+} and heliumlike Ar^{16+} are shown in Fig.10 by the solid curves. The density of Ar^{17+} in the outer regions of the plasma is several orders of magnitude higher than would be the case for coronal equilibrium [16], allowing radiative recombination to dominate the population of the upper levels of the Ar^{16+} lines in the very cold regions.

As a point of reference, consider the resonance and forbidden line brightness profiles from the bottom of the plasma, with the drift down. The measured and calculated brightness profiles are shown in Fig.11, and the agreement is very good. This agreement is taken as support of the collisional-radiative model, the measured electron temperature and density profiles, the calculated argon charge state density profiles and the modelled impurity transport. The calculated brightness profiles are not extremely sensitive to the exact form of the impurity transport coefficients. Shown in Fig.12 are the brightness profiles from the top of the plasma with the drift down, where the perturbed Ar^{17+} density profile from Fig.10 has been used; the large bumps between 18 and 22 cm are well fit by the perturbation in the Ar^{17+} density profile. In fact, the perturbation to the charge state density profile was

determined by adjusting the calculated brightness profiles to match the observed profiles. This density perturbation is about a factor of 8, near the last closed flux surface. It would be very difficult to account for this brightness asymmetry with an asymmetry in the electron temperature, because the radiative recombination rate [20] is a weak function of temperature. From Thomson scattering measurements at +19.4 cm (r=16 cm) and −22.6 cm (r=19 cm), there is no indication of an up-down electron temperature or density asymmetry, although in principle there could be an electron density asymmetry outside of 19 cm. However, the most reasonable explanation of the observed brightness asymmetry is an up-down impurity density asymmetry, since there are aspects of the measurements in qualitative agreement with the predictions of neo-classical impurity transport theory [6,2,7,8]. The up-down impurity enhancement is in the opposite direction from the ion $\mathbf{B}\times\nabla\mathbf{B}$ drift direction, and switches direction when the magnetic field is reversed. This impurity asymmetry is independent of the location of the X-point; the asymmetry did not change with the X-point located in either the top or bottom of the machine.

A quantitative comparison with the predictions of neo-classical impurity transport will now be given. In all treatments, the impurity density is taken to be of the form $n_I + \tilde{n}_I \sin\theta$, where θ is the poloidal angle measured from the midplane. In the discussions of Refs.[6 and 2], it is assumed that impurities are only present in trace quantities ($\alpha \equiv n_I Z_I{}^2/n_i \ll 1$), the impurities are in the Pfirsch-Schlüter regime ($\nu_{*I} \equiv \nu_{II}/(\epsilon^{3/2}\omega_{tI}) \gg 1$), the plasma has large aspect ratio (R/a $\gg$ 1) and is circular, and that the perturbation is relatively small ($\tilde{n}_I/n_I \leq .3$). (For perturbations with a $\sin\theta$ dependence, $\tilde{n}_I/n_I \leq 1$, or the impurity density will go negative.) For the discharge of Fig.1 at .5 s, $\alpha \sim .06$ ($n_{Ar} = 2.7\times10^{10}$ cm^{-3}) and ν_{*I} is everywhere ≥ 50, so the first two conditions are satisfied. The aspect ratio of Alcator C-Mod is ~ 3 and for the discharge of Fig.1, the elongation was 1.6, so the other conditions are marginally met. From Eq.2 of Ref.[2], the impurity density perturbation is found to be, for the Pfirsch-Schlüter regime,

$$\frac{\tilde{n}_I}{n_I} \approx 1.76 \times 10^{-7} \frac{n_i q^2}{T_i^{3/2}} \left(\frac{-n_i'}{n_i} + \frac{T_i'}{17 T_i}\right) \quad (1)$$

with n_i, the background deuteron density, in cm^{-3}, T_i in eV, $Z_I = 17$ for argon, B_T=5.3 T, q is the safety factor and primes indicate spatial derivatives. (This expression differs from Eq.13 of Ref.[6] by a factor of $\sqrt{2}$.) The q profile for the discharge of Fig.1 at .5 s, determined from EFIT, may be approximated by $q(r) \simeq \exp(\frac{r}{17.3cm})^{2.65} - .075$. The spatial profile of the neo-classical impurity perturbation of Eq.1 may be calculated from the profiles of Figs.8 and 9 and the q profile, assuming $n_i = n_e$, and is shown in Fig.13 by the solid curve. The calculated perturbation grows very rapidly past 10 cm, and continues to values beyond the validity of the treatment. A non-linear extension of the calculation leading to Eq.1, intended to be self-consistently valid for large impurity density perturbations ($\sim O(\epsilon)$), is presented in Refs.[7 and 8]. $\tilde{n}_I/n_I$, calculated from Eq.2.17c in Ref.[8], is also shown in Fig.13, by the dotted curve. These two curves are identical for radii smaller than 13 cm; the non-linear perturbation peaks at a value of .22 at 15 cm, and then decreases back to zero. The maximum allowable perturbation in the non-linear treatment has the value of ϵ. Also shown in Fig.13 is the density perturbation from Fig.10, determined from the best fit to the brightness profile of Fig.12. While the qualitative agreement between the inferred impurity density perturbation and those calculated from neo-classical theory is good (the direction of the asymmetry, and the increase with minor radius), there are quantitative differences, in that the inferred asymmetry is larger in magnitude, and occurs closer to the last closed flux surface, compared to the calculated profiles. Observed *cross* field transport [29] is known to be much larger than the neo-classical predictions, and this has not been taken into account in the above theoretical comparisons. There may also be some anomalous mechanisms at work for parallel transport. A self-consistent 2D impurity transport calculation (as in Ref.[2]) has not been performed. The calculated asymmetry is sensitive to the details of the electron density profile. The large observed asymmetry is certainly not due to the influence of neutral particles

since it was not affected by changing the X-point from the bottom to the top of the machine. Operating in the divertor configuration is not relevant for this effect since it has been observed in Alcator C and other limited devices [1,3,4]. Edge impurity source asymmetries are not relevant in the Alcator C-Mod and Alcator C cases since the observed asymmetry is due to Ar^{17+}, which must come from the plasma center.

V. Conclusions

Large up-down asymmetries in Ar^{16+} x-ray brightnesses have been observed from the edge of Alcator C-Mod plasmas, where the upper levels of the transitions are populated by radiative recombination of Ar^{17+} which has come from the plasma center. Modelling of the observed brightness profiles indicates that the brightness asymmetries can be explained by an asymmetry in the Ar^{17+} density of a factor of ~ 8, just inside the last closed flux surface. This asymmetry is in the opposite direction from the ion $\mathbf{B}\times\nabla\mathbf{B}$ drift direction, and changes direction when the direction of the toroidal magnetic field is reversed. These observations are in qualitative agreement with the predictions of neo-classical parallel impurity transport theory (in the collisional regime) in the direction of the impurity asymmetry with respect to the toroidal magnetic field direction, and in the increase of the asymmetry towards the plasma edge. The observed asymmetry, however, is larger in magnitude than the predictions, and peaks at a larger radius.

Acknowledgements

The authors would like to thank J. Irby and P. Stek for electron density measurements, A. Hubbard and P. O'Shea for electron temperature measurements, S. Wolfe for flux surface calculations, R. Watterson for Thomson scattering measurements, K. Burrell, M. Greenwald, M. Graf and K. Wenzel for useful discussions and the Alcator C-Mod operations group for expert running of the tokamak. Work supported at MIT by DoE Contract No. DE-AC02-78ET51013.

References

[1] J.L.Terry, E.S.Marmar, K.I.Chen and H.W.Moos, Phys. Rev. Lett. **39** (1977) 1615.

[2] K.Brau, S.Suckewer and S.K.Wong, Nucl. Fusion **23** (1983) 1657.

[3] K.W.Wenzel, Measurements of Injected Impurity Transport in TEXT Using Multiply Filtered Soft X-ray Detectors, Ph.D. thesis, Massachusetts Institute of Technology, Cambridge (1989).

[4] R.D.Durst, Nucl. Fusion **32** (1992) 2238.

[5] S.Regan, Soft-X-Ray Spectroscopy on the Phaedrus-T Tokamak, Ph.D. thesis, the Johns-Hopkins University, Baltimore (1995).

[6] K.H.Burrell and S.K.Wong, Nucl. Fusion **19** (1979) 1571.

[7] C.T.Hsu and D.J.Sigmar, Plasma Phys. Control. Fusion **32** (1990) 499.

[8] D.J.Sigmar et al., in Theory of Fusion Plasmas (Proc. Joint Varenna- Lausanne Int. Workshop, 1990), Editrice Compositori, Bologna (1990) 65.

[9] I.H.Hutchinson et al., Phys. Plasmas **1** (1994) 1511.

[10] J.E.Rice and E.S.Marmar, Rev. Sci. Instrum. **61** (1990) 2753.

[11] E.Källne et al., Phys. Rev. A **28** (1983) 467.

[12] E.Källne et al., Phys. Rev. Lett. **52** (1984) 2245.

[13] TFR Group et al., Phys. Rev. A **32** (1985) 2374, Phys. Rev. A **32** (1985) 3000.

[14] E.Källne et al., Nucl. Instrum. Methods B **9** (1985) 698.

[15] E.Källne et al., Phys. Scr. **31** (1985) 551.

[16] J.E.Rice, E.S.Marmar, E.Källne and J.Källne, Phys. Rev. A **35** (1987) 3033.

[17] K.J.H.Phillips et al., J. Phys. B **27** (1994) 1939.

[18] L.A.Vainshtein and U.I.Safronova, Physica Scripta **31** (1985) 519.

[19] L. A. Vainshtein and U. I. Safronova, Atomic Data and Nuclear Data Tables **21** (1978) 49.

[20] R. Mewe and J. Schrijver, Astron. Astrophys. **65** (1978) 99.

[21] R. Mewe, J. Schrijver and J. Sylwester, Astron. Astrophys. **87** (1980) 55.

[22] J.H.Irby et al., Rev. Sci. Instrum. **59** (1988) 1568.

[23] T.C.Hsu et al., Proc. 8th Joint Workshop on ECE and ECRH, IPP III/186 (1993) 409.

[24] R. A. Hulse, Nucl. Tech./Fus. **3** (1983) 259.

[25] M.A.Graf et al., Rev. Sci. Instrum. **66** (1995) 636.

[26] J.E.Rice et al., Rev. Sci. Instrum. **66** (1995) 752.

[27] L. L. Lao et al., Nucl. Fusion **25** (1985) 1611.

[28] B.Blackwell et al., in *Plasma Physics and Controlled Nuclear Fusion Reasearch 1982* Proceedings of the 9th International Conference, Baltimore, MD, Vol.II (IAEA, Vienna 1983) 27.

[29] E.S.Marmar et al., Phys. Rev. Lett. **45** (1980) 2025.

Figure Captions

Fig. 1 Time histories of the plasma current, central electron density, central electron temperature, central chord Ar^{16+} brightness and central argon density. Argon was injected at .4 s.

Fig. 2 Central chord Ar^{16+} spectrum showing the resonance line, w, the inter-combination lines, x and y, and the forbidden line, z, as well as several satellites. A synthetic spectrum is shown by the thin line.

Fig. 3 Spectra from a top viewing chord (solid) and a bottom viewing chord (dotted) from r/a $\sim$.6. A synthetic spectrum is shown by the thin line. The chordal views are shown in the inset.

Fig. 4 Spectra from a top viewing chord (solid) and a bottom viewing chord (dotted) from r/a $\sim$.9. In this case, the ion $\mathbf{B}\times\nabla\mathbf{B}$ drift was downward. A synthetic spectrum is shown by the thin line, normalized to the top spectrum.

Fig. 5 Spectra from a top viewing chord (solid) and a bottom viewing chord (dotted) from r/a $\sim$.9. In this case, the ion $\mathbf{B}\times\nabla\mathbf{B}$ drift was upward.

Fig. 6 Vertical brightness profiles for the forbidden line with the ion $\mathbf{B}\times\nabla\mathbf{B}$ drift downward (asterisks) and upward (boxes).

Fig. 7 Vertical brightness profiles for the resonance line (triangles) and forbidden line (asterisks) with the ion $\mathbf{B}\times\nabla\mathbf{B}$ drift downward, for Alcator C plasmas.

Fig. 8 Electron and ion temperature profiles at .5 s for a series of discharges identical to that shown in Fig.1. The thin solid line is an analytic fit to the ion temperature data.

Fig. 9 Measured electron density profile (thick solid curve) at .5 s for a shot

similar to that shown in Fig.1, and an analytical approximation (thin curve). The calculated total argon density profile ($\times 1000$) is shown by the dash-dot-dot-dot curve.

Fig. 10 Calculated argon density profiles for heliumlike Ar^{16+} and hydrogenlike Ar^{17+} charge states. The dotted bump at $\sim$21 cm is a modelled perturbation.

Fig. 11 Measured brightness profiles of the resonance line (triangles) and forbidden line (asterisks), and the calculated profiles from the bottom of the plasma with the drift down.

Fig. 12 Measured brightness profiles of the resonance line (triangles) and forbidden line (asterisks), and the calculated profiles, including the perturbed Ar^{17+} density profile of Fig.10, from the top of the plasma with the drift down.

Fig. 13 Calculated $\tilde{n}_I/n_I$ from the treatment of Ref.(2) (solid) and the treatment of Ref.(8) (dotted), compared to the inferred impurity density perturbation (dash-dot-dot-dot) of Fig.10.

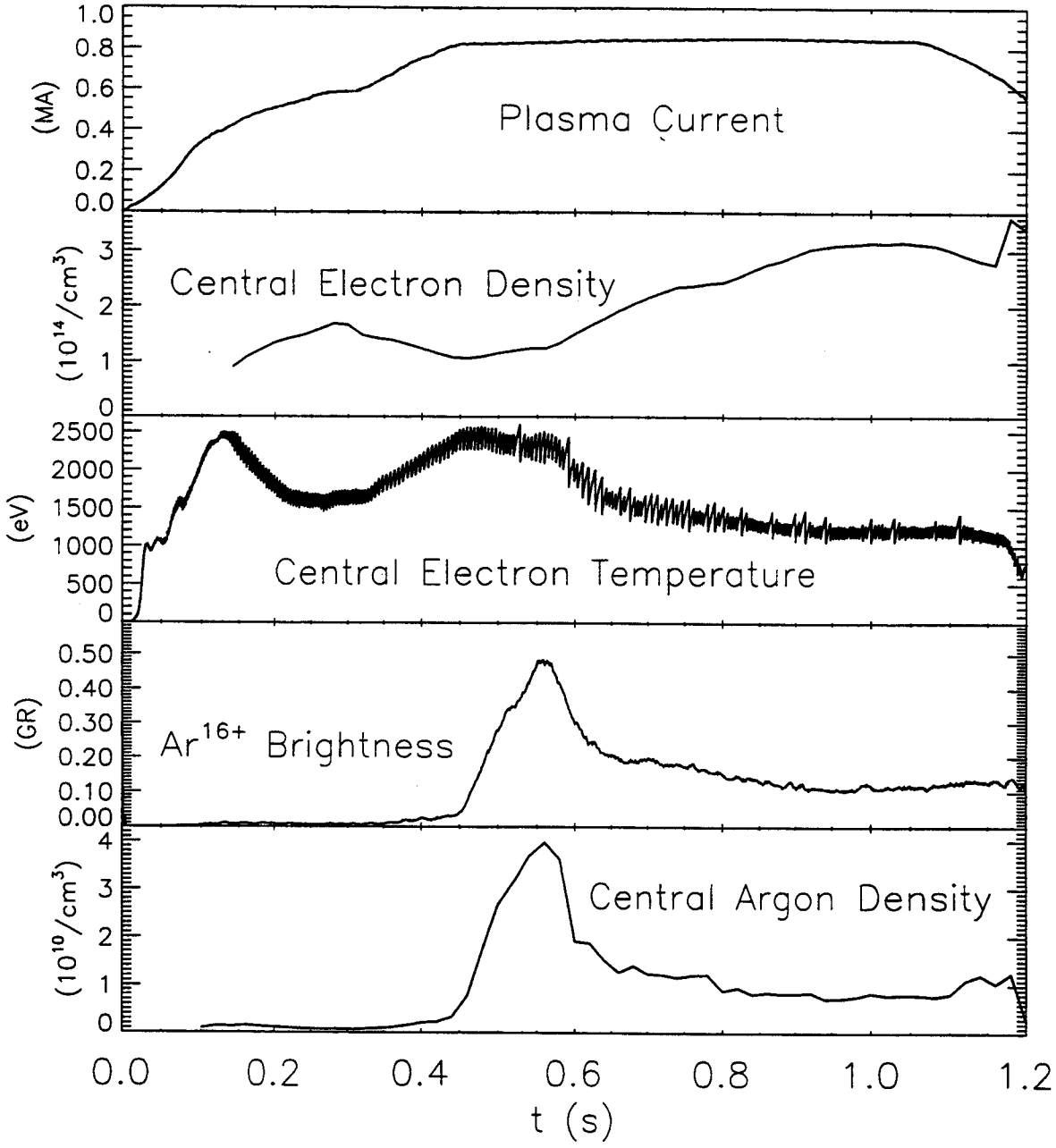
Plasma Current
(MA)
Central Electron Density
(10^14/cm^3)
Central Electron Temperature
(eV)
Ar^16+ Brightness
(GR)
Central Argon Density
(10^10/cm^3)
t (s)

Figure 1

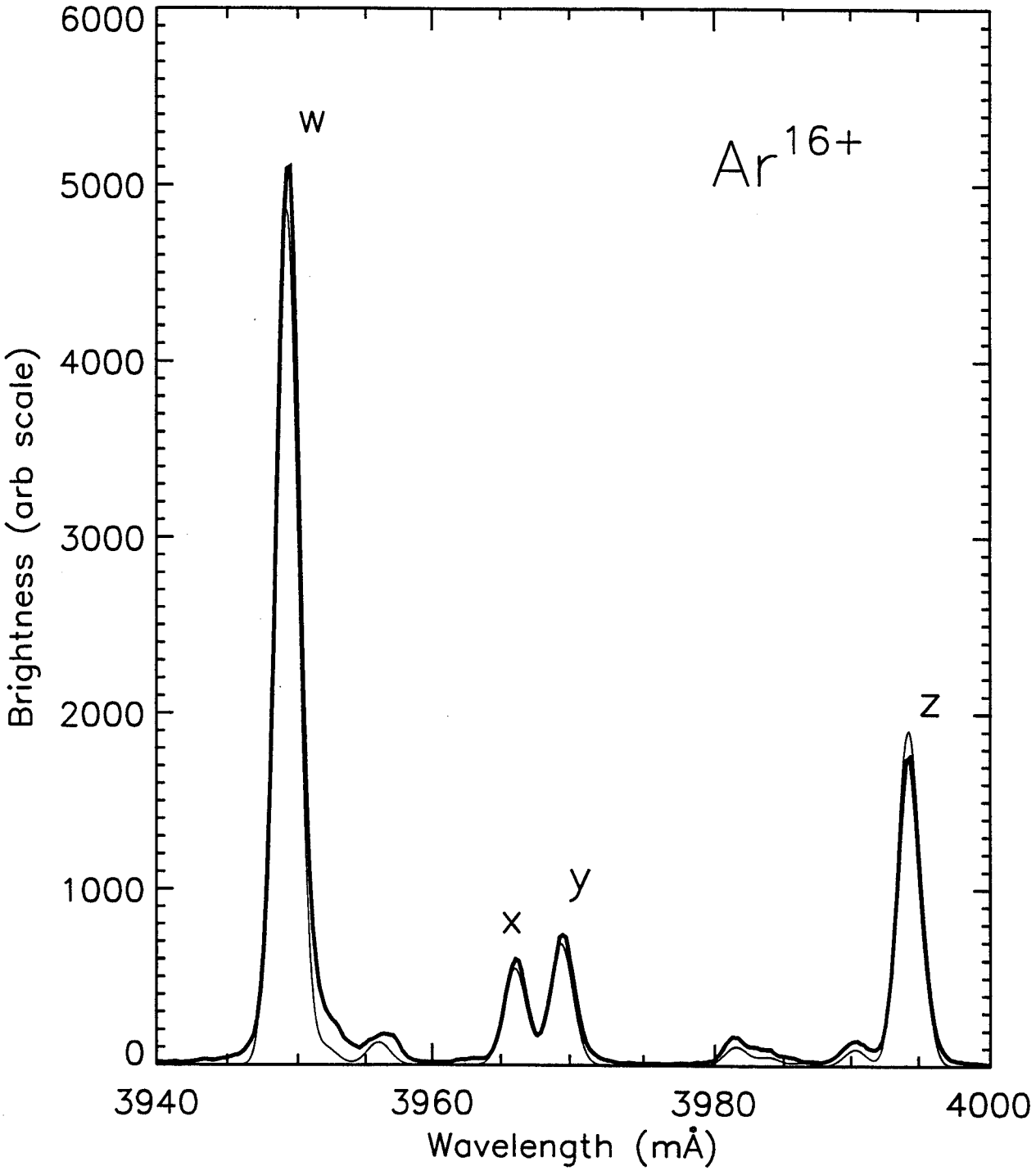
6000
5000
4000
3000
2000
1000
0
Brightness (arb scale)
w
x
y
z
Ar16+
3940
3960
3980
4000
Wavelength (mÅ)

Figure 2

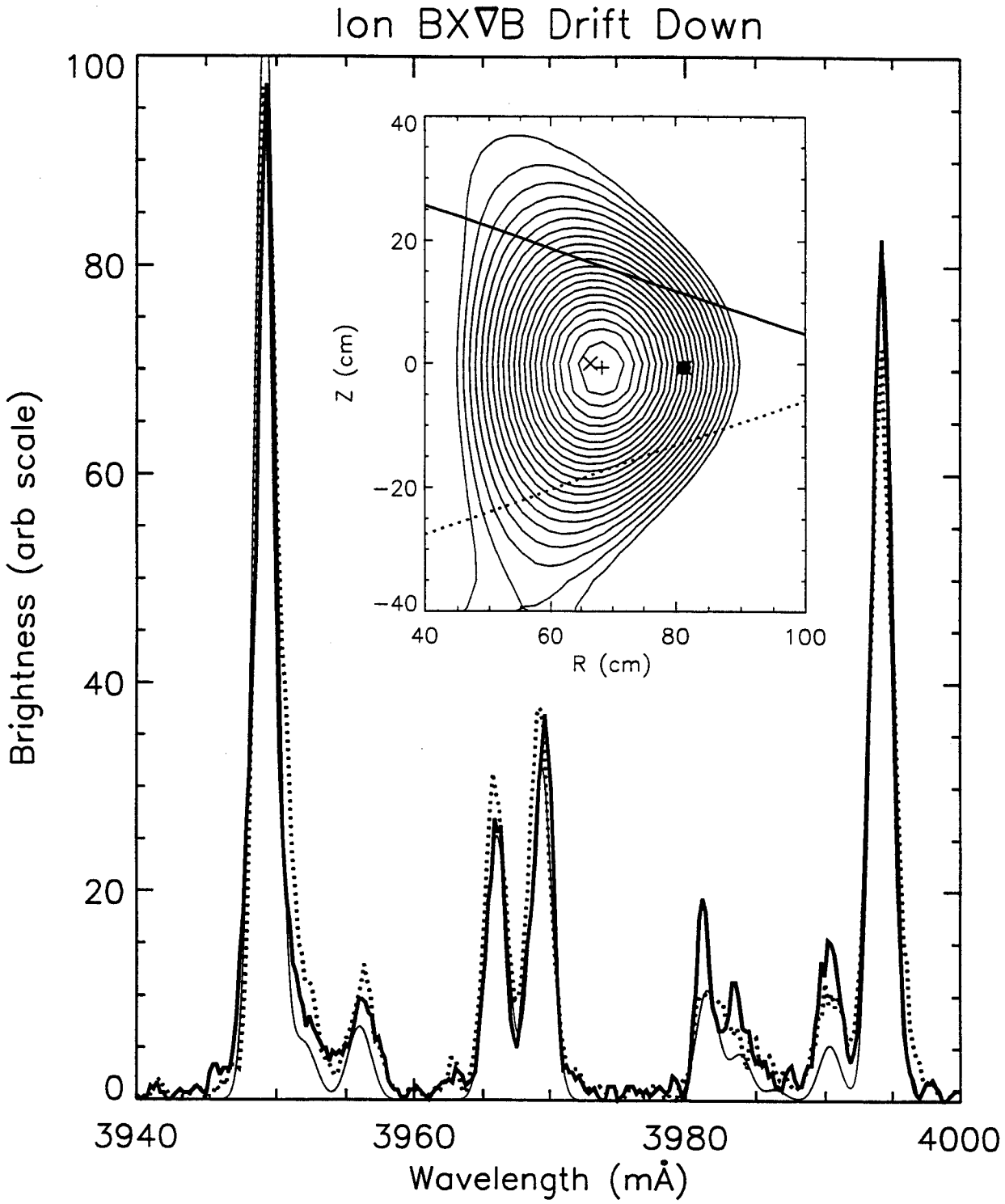
Ion BX∇B Drift Down
Brightness (arb scale)
Wavelength (mÅ)
Z (cm)
R (cm)

Figure 3

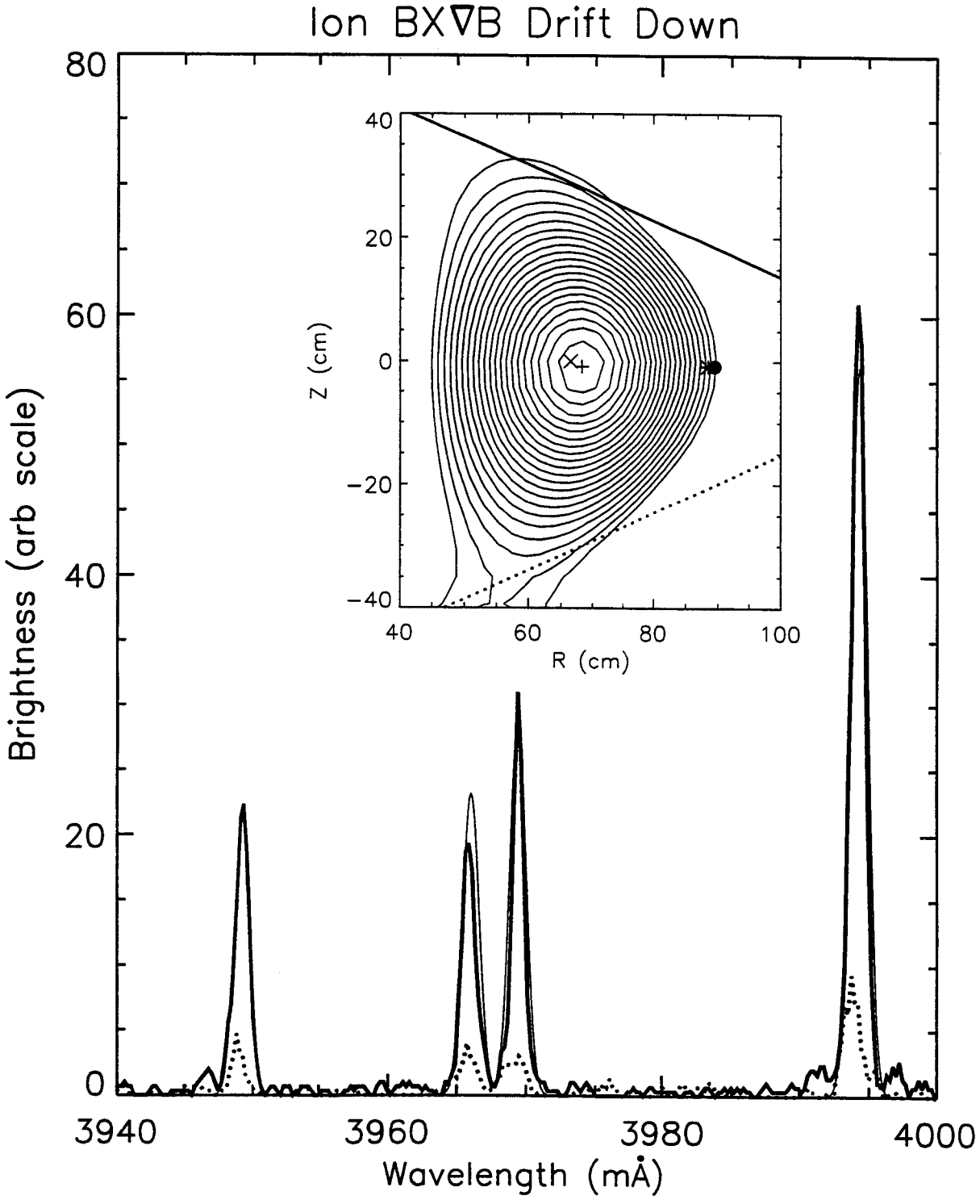
Ion BX∇B Drift Down
Brightness (arb scale)
Wavelength (mÅ)
Z (cm)
R (cm)
0
20
40
60
80
3940
3960
3980
4000
−40
−20
0
20
40
60
80
100

Figure 4

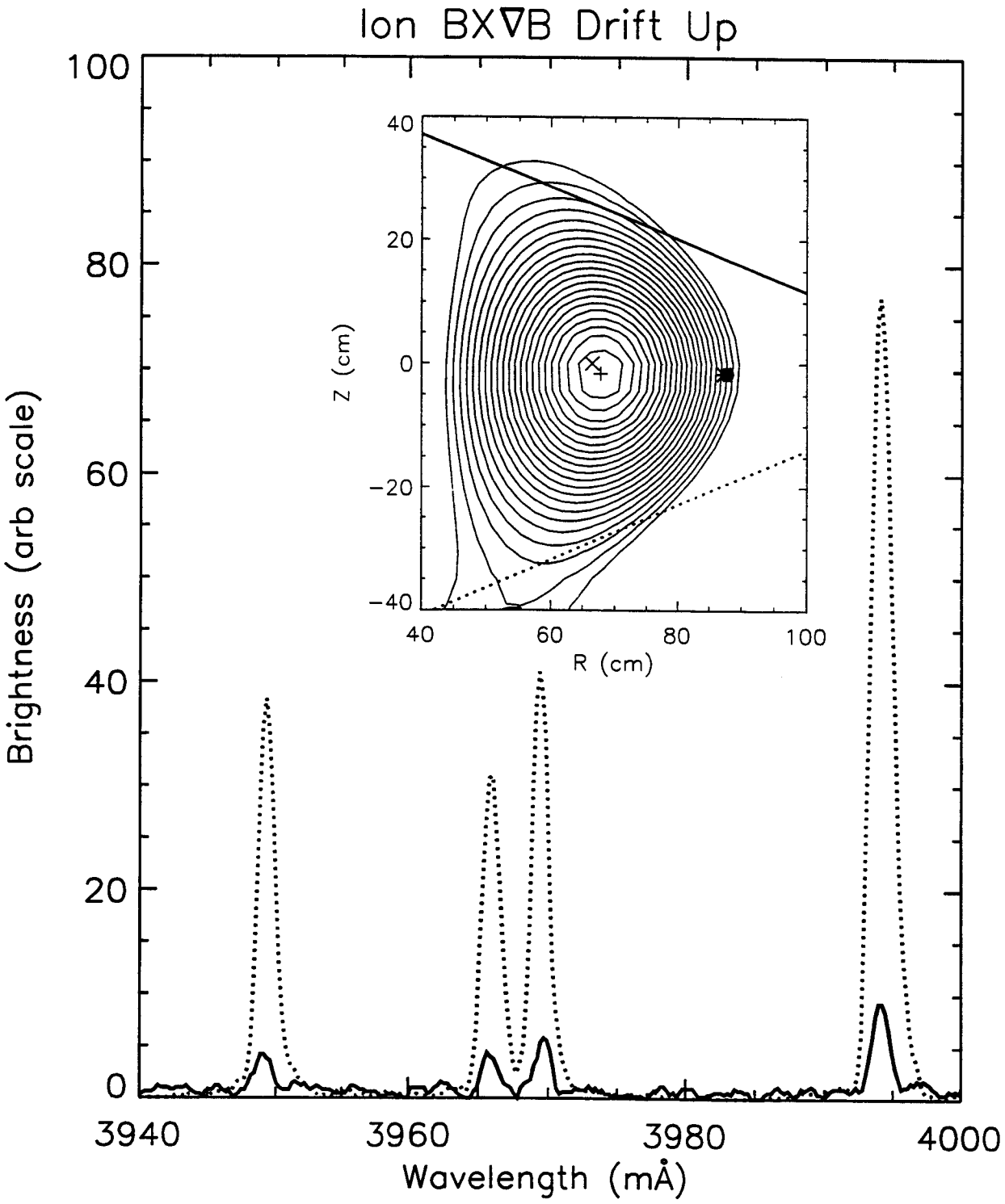

Figure 5

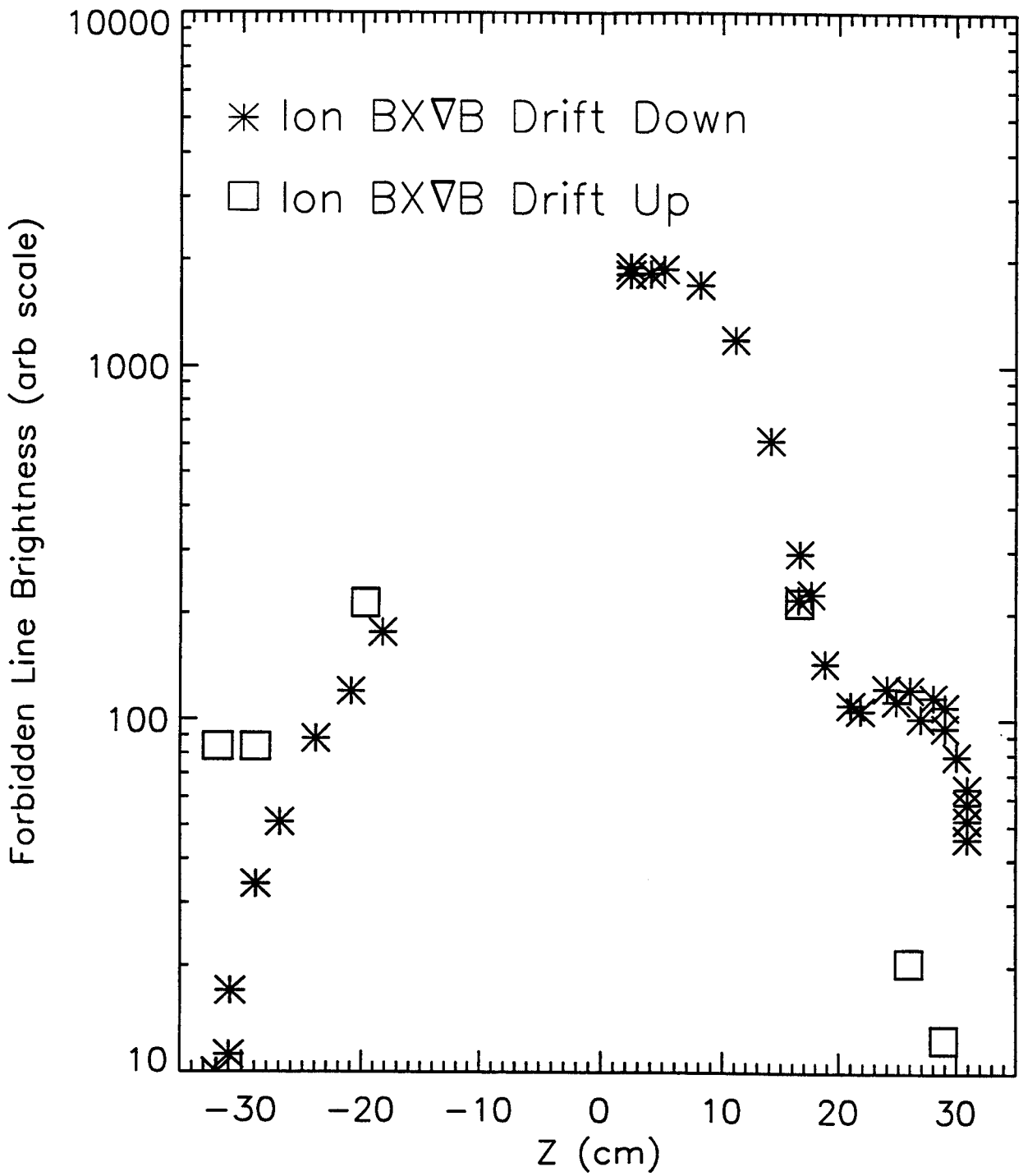
10000
1000
100
10
Forbidden Line Brightness (arb scale)
* Ion BX∇B Drift Down
□ Ion BX∇B Drift Up
−30
−20
−10
0
10
20
30
Z (cm)

Figure 6

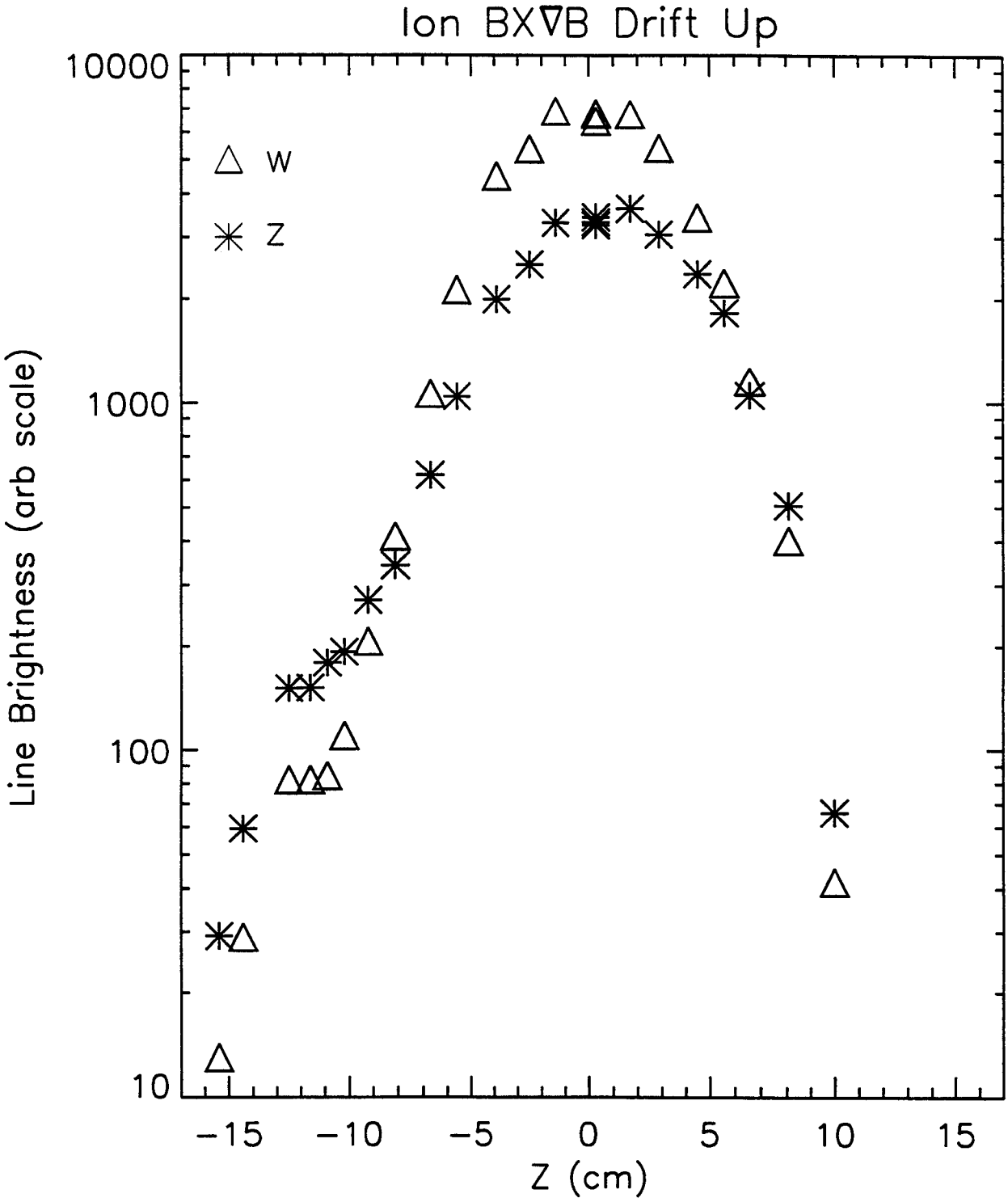
Ion BX∇B Drift Up
10000
1000
100
10
Line Brightness (arb scale)
W
Z
−15
−10
−5
0
5
10
15
Z (cm)

Figure 7

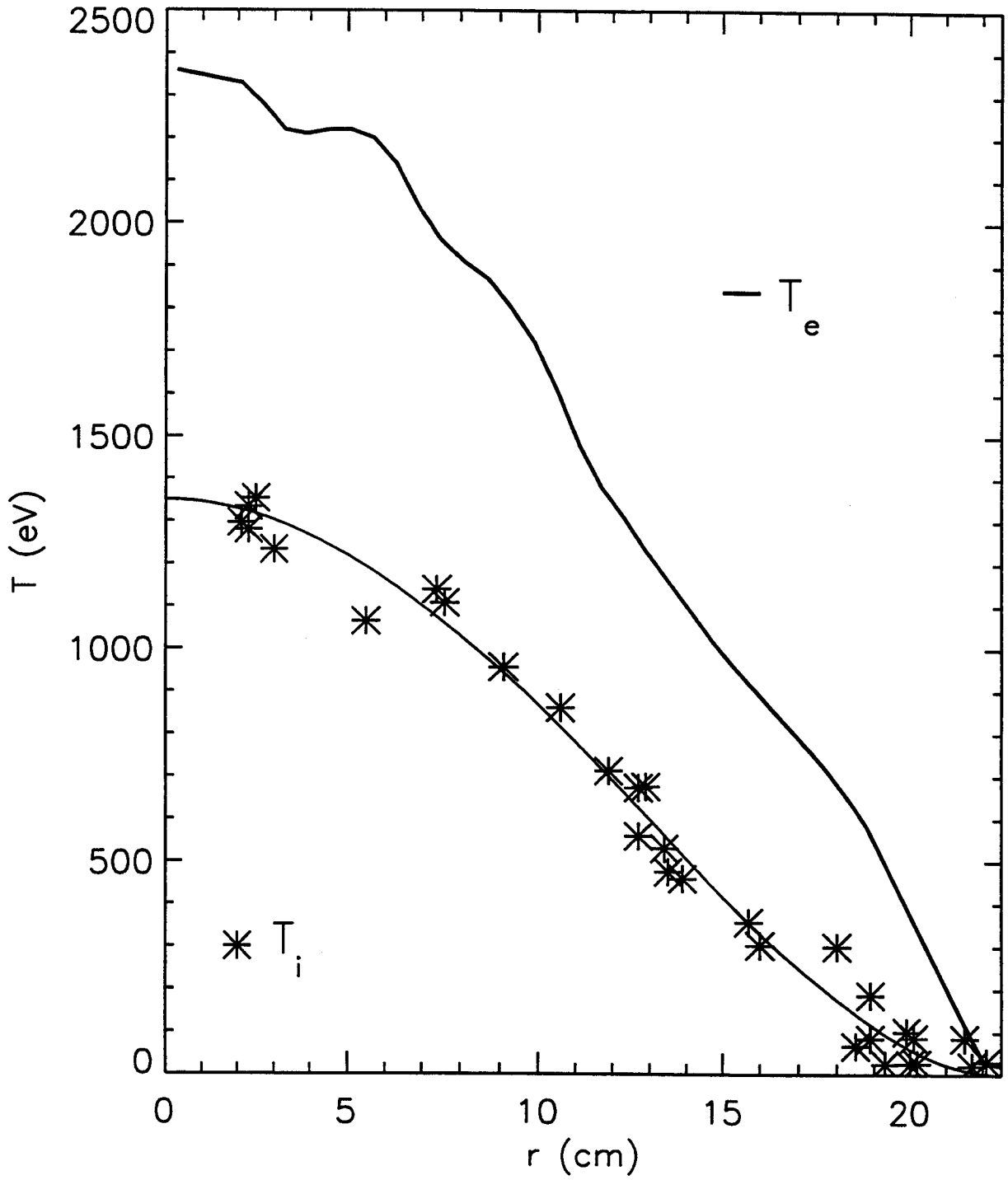

Figure 8

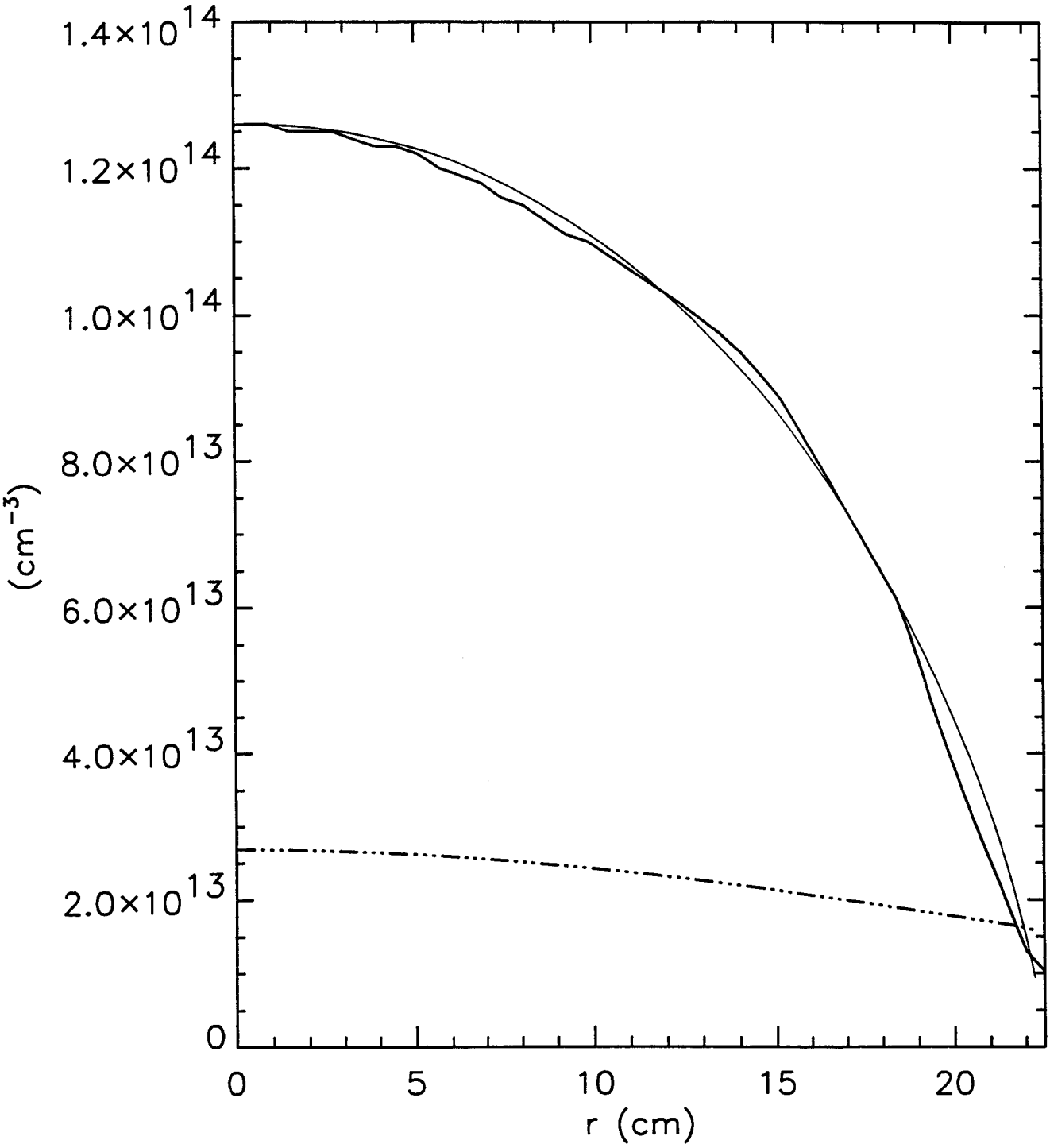
1.4×10^14
1.2×10^14
1.0×10^14
8.0×10^13
6.0×10^13
4.0×10^13
2.0×10^13
0
(cm^-3)
0
5
10
15
20
r (cm)

Figure 9

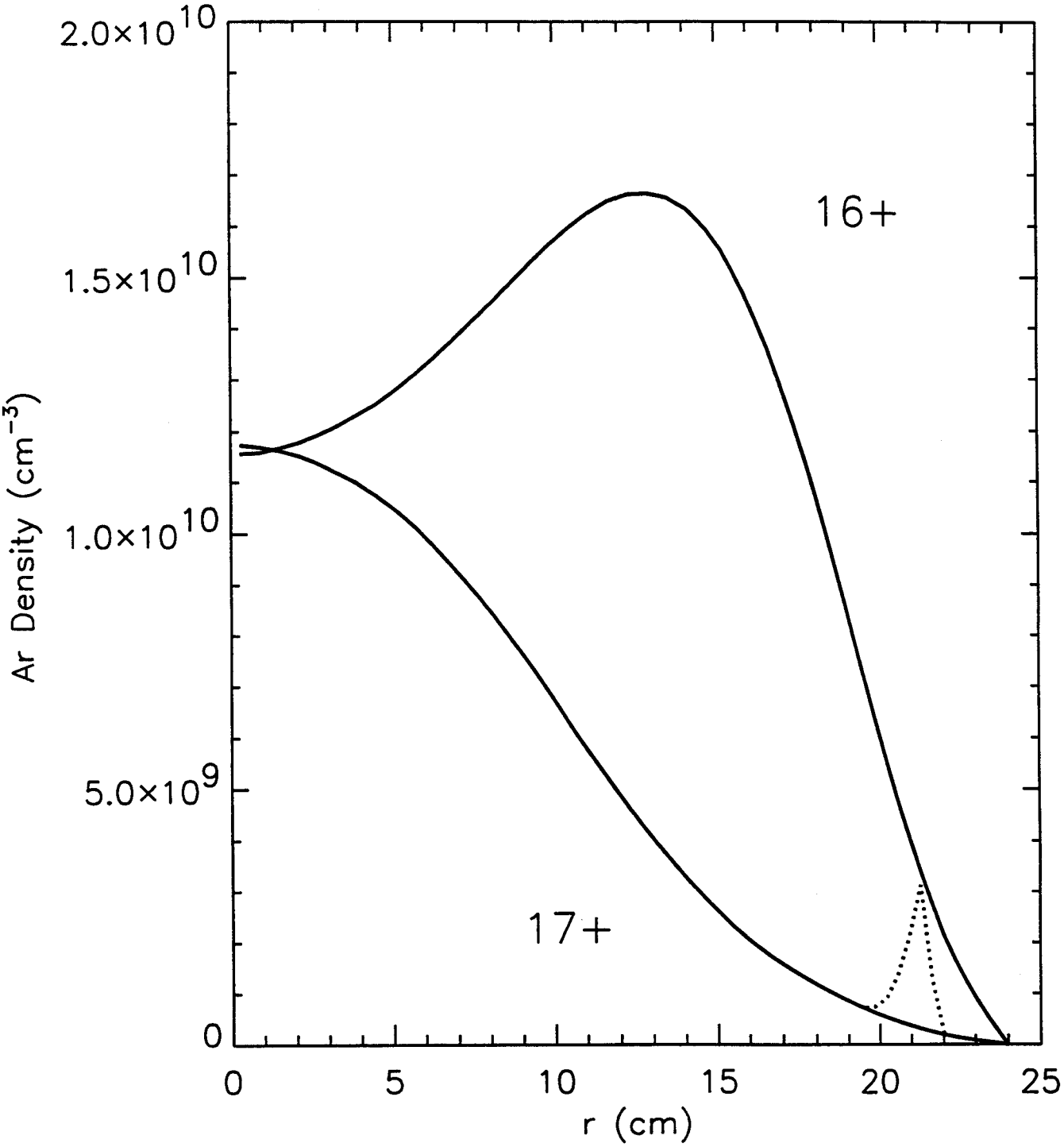
2.0×10^10
1.5×10^10
1.0×10^10
5.0×10^9
0
Ar Density (cm^-3)
16+
17+
0
5
10
15
20
25
r (cm)

Figure 10

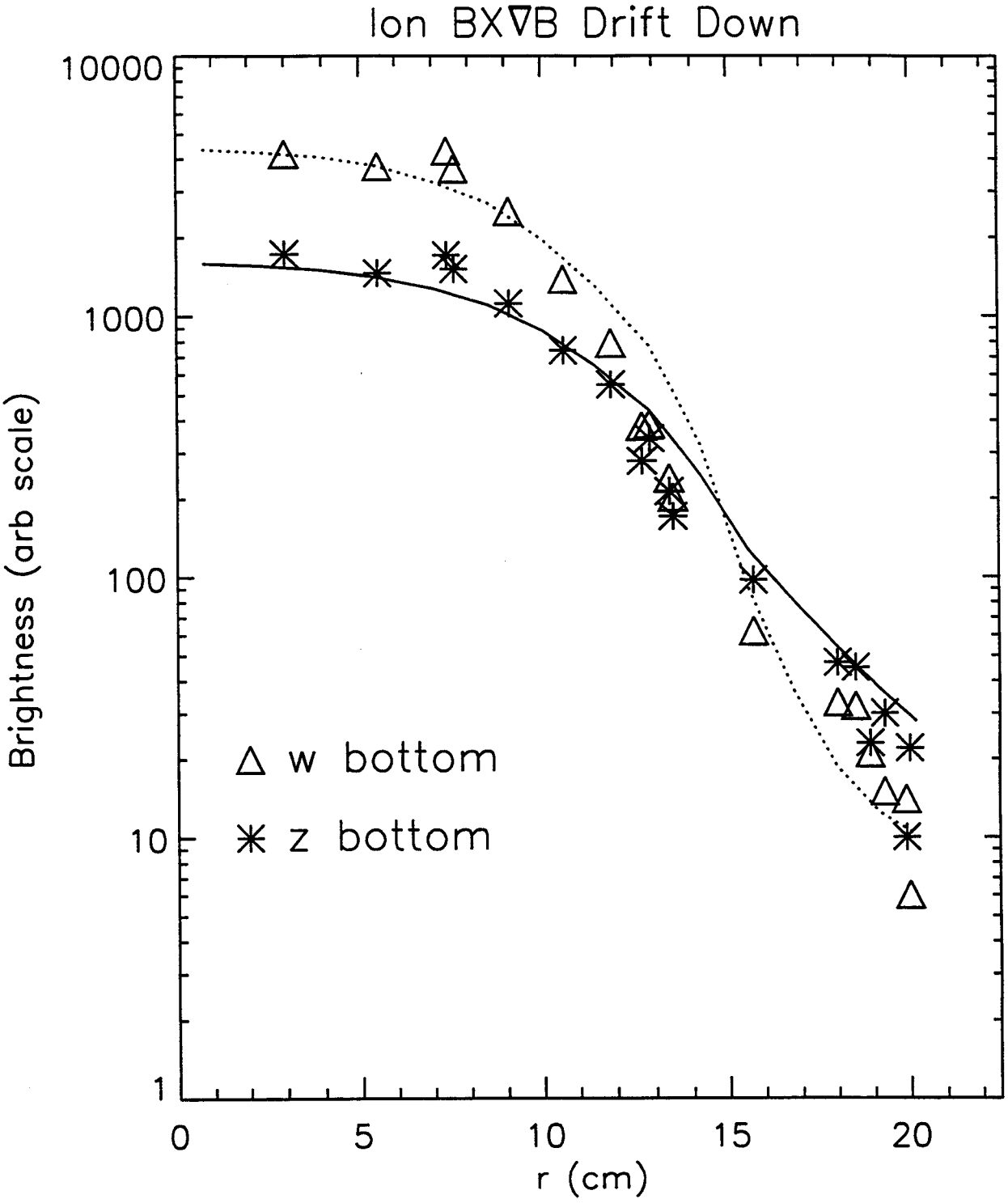
Ion BX∇B Drift Down
10000
1000
100
10
1
Brightness (arb scale)
△ w bottom
✳ z bottom
0
5
10
15
20
r (cm)

Figure 11

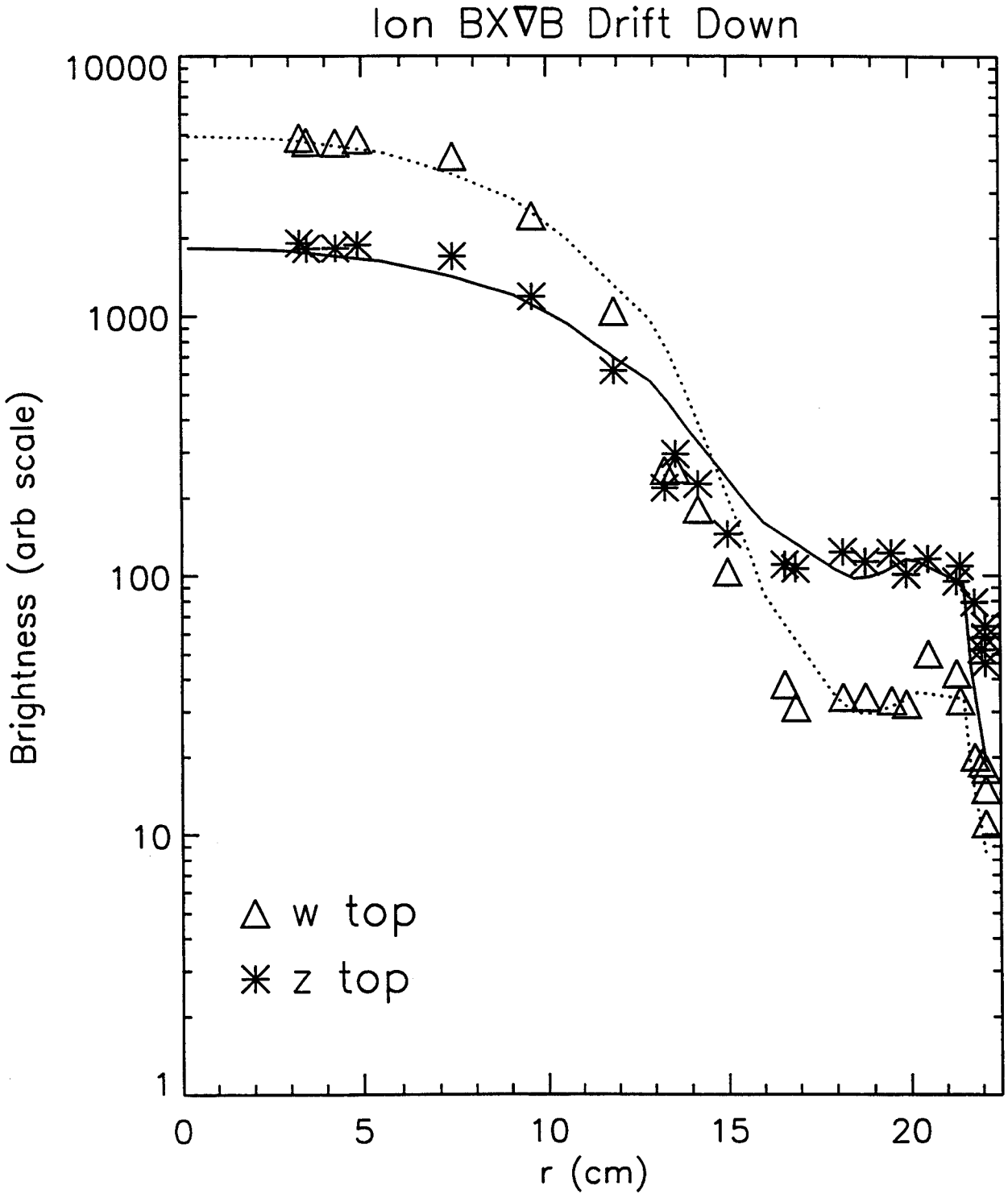
Ion BX∇B Drift Down
10000
1000
100
10
1
Brightness (arb scale)
0
5
10
15
20
r (cm)
△ w top
✳ z top

Figure 12

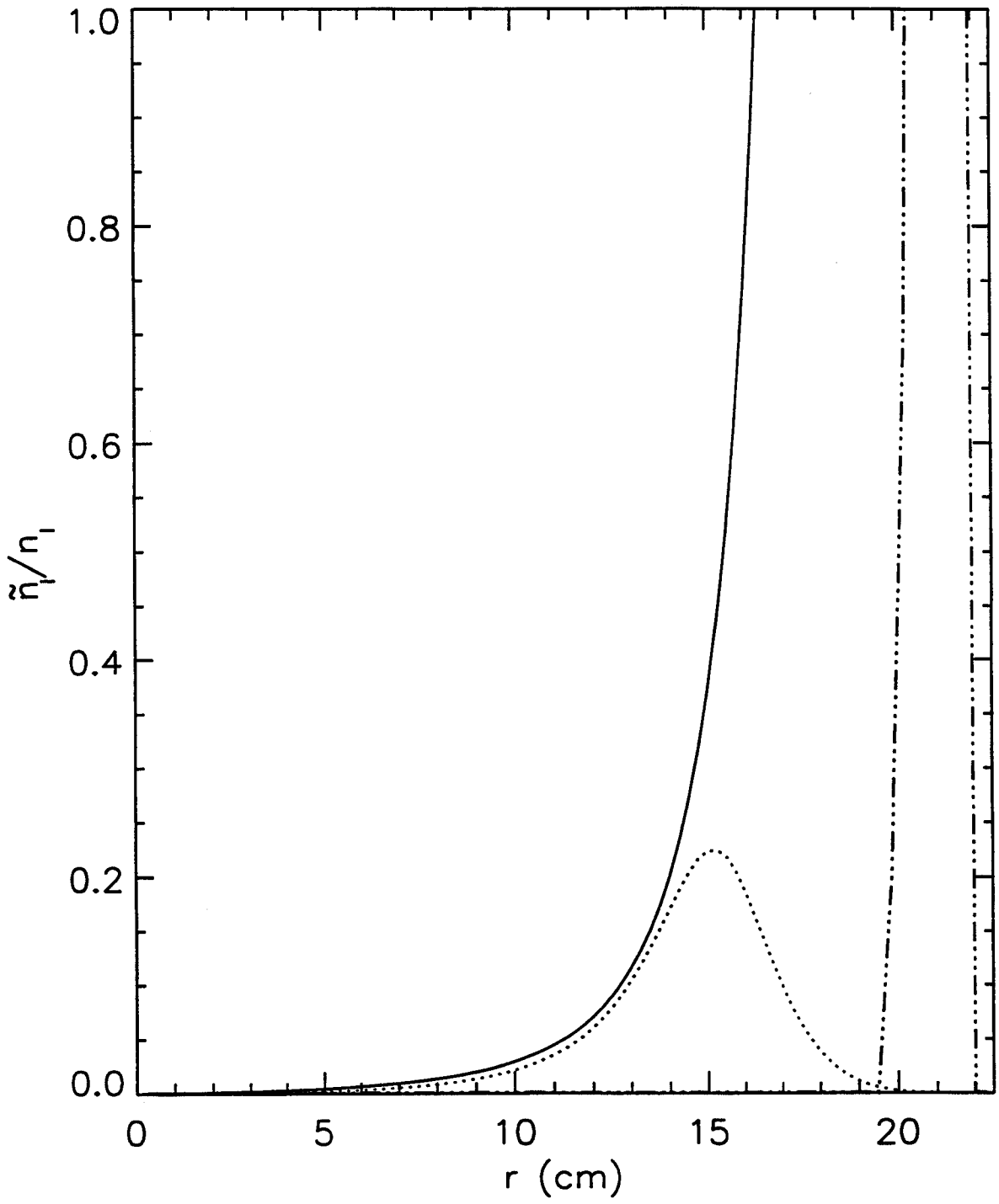

Figure 13